Journal of Magnetism and Magnetic Materials 454 (2018) 237–242

Contents lists available at ScienceDirect

Journal of Magnetism and Magnetic Materials

journal homepage: www.elsevier.com/locate/jmmm

Research articles

Interaction between the localized states in graphene

Angsula Ghosh [a,b,*], H.O. Frota [a]

[a] Department of Physics, Federal University of Amazonas, 69077-000 Manaus, AM, Brazil
[b] São Paulo State University, Institute for Theoretical Physics, São Paulo, SP, Brazil

ARTICLE INFO

Article history:
Received 27 October 2017
Received in revised form 5 January 2018
Accepted 13 January 2018

Keywords:
Graphene
Adatoms
Phase transition

ABSTRACT

The formation of the localized magnetic moments is studied due to the presence of two-impurities in the two sublattices of a single-layer graphene sheet. The interaction between two similar magnetic impurities and also the hybridizations are decisive in determining the boundary between the magnetic and the non-magnetic states. A strong chemical potential dependence of the above phase boundary is evident. An anomalous scaling of the boundary separating the above regions is more pronounced in the two-impurity case when compared to that of the single impurity.

1. Introduction

The pioneering work of Andre Geim and Kostya Novoselov [1] has triggered a huge interest in the scientific community to study graphene, mainly motivated by their unusual electronic properties, such as the behavior of non-massive chiral Dirac fermion at low excitation energies. The high-electron mobility in graphene and its planar structure make it suitable for applications in nanoscience and nanotechnology leading to a new era of carbon-based electronics.

Graphene, a two-dimensional allotrope of carbon with the sp^2 hybridization state is distributed in a hexagonal lattice formed by two interpenetrating triangular sublattices, A and B. In the lattice plane, the s and p orbitals of the carbon atom form covalent bonds and thus provide a high mechanical strength to graphene. The remaining p orbitals of the carbon atoms in each sublattice, in the direction perpendicular to the plane of the lattice, hybridize, forming a conduction and a valence energy bands, known as π^* and π bands, respectively. The hexagonal distribution results in two bands that touch each other at two high-symmetry points in the Brillouin zone, K and K', known as Dirac points, thereby leading to a zero gap semiconductor. Around these points the dispersion relation is given by $E = \pm\hbar v_F \mid \vec{k} \mid$, with the energy E varying linearly as a function of the moment $\vec{k}$, where $\hbar$ is the reduced Planck constant and v_F is the Fermi velocity. Hence, it is similar to the dispersion relation of the photon, with the speed of light c playing the role of the velocity of the electrons in the Fermi level of graphene. As a two-dimensional Dirac fermion system, graphene presents unconventional and interesting electronic behavior. For instance, graphene shows a minimum conductivity of about e^2/h, an anomalous quantum Hall effect and a nonzero cyclotron mass m_c described by $E = m_c v_F^2$, although from the linear spectrum of fermion in graphene it would be zero. This similarity with Dirac fermions enables the prediction of the properties of the charge carriers in graphene from the relativistic Dirac equation, such as tunneling through a potential barrier without any reflection, which is known as Klein's paradox.

Impurity states are regarded as important contributors to the unusual and singular properties of graphene [2,3]. In the last few years there has been an increased attention to study the effect of magnetic adatom in a pristine graphene due to its potential use in spintronics. Doping with magnetic impurities could envisage the creation of local spins in graphene including the possibility of opening a gap. Recent progress in scanning tunneling microscopy made it possible to position adatoms in graphene and image the impurity states with high spatial resolution [4]. Various studies have been performed to characterize the necessary conditions under which the transition metal adatom on graphene can form localized magnetic moment. A systematic first-principles study of transition metals from Sc to Zn, including nonmagnetic adatoms Cu and Au, embedded in graphene has also been performed [5]. Isolated hydrogen atoms absorbed on graphene are predicted to induce magnetic moments [6]. Recently, two identical impurities on a zigzag nanoribbon has been studied to demonstrate that the

* Corresponding author at: Department of Physics, Federal University of Amazonas, 69077-000 Manaus, AM, Brazil.
E-mail address: angsula@ufam.edu.br (A. Ghosh).

https://doi.org/10.1016/j.jmmm.2018.01.033
0304-8853/

chemical potential and the spin-orbit coupling could drive the transition of the local-spin exchange from ferromagnetism to antiferromagnetism [7]. The impurity interaction control via the adjustment of the chemical potential has also been considered to observe that a weak repulsion is observed when the two atoms reside on the same sublattice and a stronger attraction when they are on different sublattices [8]. Double impurities have also been considered for local density of states calculations [9].

The presence of a magnetic adatom in a metal has been successfully studied using the Anderson model [10,11], which recently has been applied also to study magnetic moment formation in graphene [7,12,13]. Depending on the relation between the constitutive parameters of this model, the adatom orbital can be empty, single or doubly occupied. In particular, for temperatures higher than the Kondo temperature [14], there is a formation of local magnetic moment when the adatom and the conduction electrons are weakly hybridized and the Coulomb interaction between the electrons in the adatom orbital is greater than their binding energy. Moreover, for hybridization energy higher than the electron binding energy the orbital presents the valence fluctuation regime [14]. It has been observed that the coupling of a adatom to a graphene sublattice results in a much easier formation of magnetic moment due to the anomalous broadening of the electronic levels of the adatom [14]. In the present work we study the formation of the local magnetic moments due to the presence of two similar magnetic impurities in pristine graphene. The formation of the magnetic states in the single-layer graphene can be seen to depend on the interaction between the two impurities as observed in metals [11]. Moreover, the anomalous scaling of the magnetic boundary separating the magnetic and non-magnetic states alike the single-impurity in graphene continues to exist. The chemical-potential driven phase transition is also considered.

2. The model

The model Hamiltonian of graphene with two impurities hybridized with two sublattices of a single-layer graphene as shown in Fig. 1 is written as

$$H = H_{TB} + H_f + H_V \tag{1}$$

where H_{TB} is the tight binding Hamiltonian of the graphene, H_f is the impurity Hamiltonian, H_V is the hybridization of the adatom localized states with the graphene conduction electrons.

The tight binding Hamiltonian is given by

$$H_{TB} = -t\sum_{\langle i,j\rangle\sigma,l}\left[a^{\dagger}_{\sigma}(R_i)b_{\sigma}(R_j) + H.c.\right] \tag{2}$$

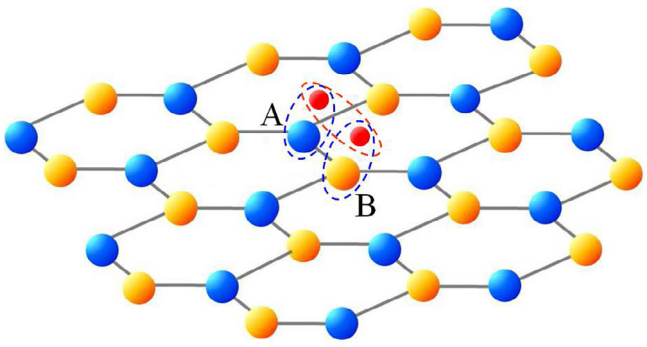

Fig. 1. Schematic diagram of the lattice structure of single layer graphene with two impurity atoms, each one coupled to the lattices A and B, respectively, and to each other.

where the operator $a_{\sigma}(R_i)$ ($b_{\sigma}(R_j)$) annihilates a state with spin σ at the position $R_i(R_j)$ on the sublattice A(B), $\langle i,j\rangle$ stands for summation over the nearest neighbors and the parameter t is the nearest neighbor hopping energy. In momentum space, we have

$$H_{TB} = -t\sum_{\mathbf{k},\sigma}\left[\phi(\mathbf{k})a^{\dagger}_{\mathbf{k},\sigma}b_{\mathbf{k},\sigma} + \phi(\mathbf{k})b^{\dagger}_{\mathbf{k},\sigma}a_{\mathbf{k},\sigma}\right] \tag{3}$$

where $\phi(\mathbf{k}) = \sum_{\delta}e^{i\mathbf{k}.\bar{\delta}_i}$ with $\bar{\delta}_1 = a(\hat{x}/2 + \sqrt{3}/2\hat{y})$, $\bar{\delta}_2 = a(\hat{x}/2 - \sqrt{3}/2\hat{y})$ and $\bar{\delta}_3 = -a\hat{x}$ as the nearest neighbor vectors. a is the lattice parameter. Diagonalizing the Hamiltonian (3) one generates two bands $\epsilon_{\pm}(\mathbf{k}) = \pm t|\phi(\mathbf{k})|$, which can be linearized around the Dirac points $\mathbf{K}$ at the corners of the Brillouin zone: $\epsilon_{\pm}(\mathbf{K}+\mathbf{q}) \sim \pm v_F|\mathbf{q}|$, where $v_F = 3ta/2$ is the Fermi velocity of the Dirac electrons.

The impurity Hamiltonian is described by

$$H_f = \sum_{\sigma}\epsilon_f(f^{\dagger}_{a\sigma}f_{a\sigma} + f^{\dagger}_{b\sigma}f_{b\sigma}) + U(n_{a\uparrow}n_{a\downarrow} + n_{b\uparrow}n_{b\downarrow}) + V_{ab}(f^{\dagger}_{a\sigma}f_{b\sigma} + f^{\dagger}_{b\sigma}f_{a\sigma}), \tag{4}$$

where $f^{\dagger}_{a\sigma}$ ($f^{\dagger}_{b\sigma}$) is the creation operator of a state with a spin $\sigma = \uparrow,\downarrow$ at the impurity of the sublattice A(B), $n_{a\sigma} = f^{\dagger}_{a\sigma}f_{a\sigma}$ and $n_{b\sigma} = f^{\dagger}_{b\sigma}f_{b\sigma}$ are the occupation number operators for the impurities in the sublattices A and B respectively. ϵ_f is the energy of the adatom electron, and U is the Coulomb interaction due to the double occupancy of an energy level in the adatom. The impurities interact with each other via the potential V_{ab}. For simplicity we adopt a mean-field approximation to the electronic correlations of the impurities, $Un_{\alpha\uparrow}n_{\alpha\downarrow} = U\sum_{\sigma}\langle n_{\alpha-\sigma}\rangle f^{\dagger}_{\alpha\sigma}f_{\alpha\sigma} - U\langle n_{\alpha\uparrow}\rangle\langle n_{\alpha\downarrow}\rangle$, where $\alpha = a, b$. Hence, the impurity Hamiltonian can be rewritten as

$$H_f = \sum_{\sigma}(\epsilon_{a\sigma}f^{\dagger}_{a\sigma}f_{a\sigma} + \epsilon_{b\sigma}f^{\dagger}_{b\sigma}f_{b\sigma}) + V_{ab}f^{\dagger}_{a\sigma}f_{b\sigma} + V^{\dagger}_{ab}f^{\dagger}_{b\sigma}f_{a\sigma}$$

where $\epsilon_{a\sigma} = \epsilon_f + U\langle n_{a-\sigma}\rangle$ and $\epsilon_{b\sigma} = \epsilon_f + U\langle n_{b-\sigma}\rangle$. The impurity orbital of the sublattice B is sited at the origin of the sublattice B and that of the sublattice A is at $\mathbf{r}_a = a\hat{r}$.

The hybridization of the impurity orbitals is given by

$$H_V = \frac{V_a}{\sqrt{N_a}}\sum_{\mathbf{k}}e^{ik_x a}a^{\dagger}_{k\sigma}f_{a\sigma} + \frac{V_b}{\sqrt{N_b}}\sum_{\mathbf{k}}b^{\dagger}_{k\sigma}f_{b\sigma} + H.c, \tag{5}$$

where N_a (N_b) denotes the number of atoms in the sublattice a (b), V_a and the V_b are the hybridization interactions of the impurities in the sublattices A and B respectively.

3. The formalism

The formation of a magnetic moment depends on the occupation of the two spin states of the impurities. The localized moment is formed when $n_{\alpha\uparrow} \neq n_{\alpha\downarrow}$. The interaction between the impurities V_{ab} is important to understand the relation between the localized states of the single-layer graphene. The self-consistent calculations of the density of states in the presence of the hybridization and V_{ab} is performed for the determination of the occupation of the impurities. The occupation of the impurity level can be determined by

$$n_{\alpha\sigma} = \frac{1}{2\pi}\int_{-\infty}^{\mu}d\omega A_{\alpha f\sigma}(\omega) \tag{6}$$

where the spectral function is given by

$$A_{\alpha f\sigma}(\omega) = -2\Im G^{R}_{\alpha f\sigma}(\omega). \tag{7}$$

The single particle retarded Green's function [15–18] of the f electrons is $G^{R}_{\alpha f\sigma}(t) = -i\theta(t)[f_{\alpha\sigma}(t), f_{\alpha\sigma}(t)]$ and the Fourier transform of that of the sublattice b can be written as

$$G^R_{bf\sigma}(\omega) = \left[\omega - \epsilon_{b\sigma} - \Sigma_{bb}(\omega) - \frac{(\lambda_{ab}+V_{ab})(\lambda_{ba}+V_{ba})}{\omega - \epsilon_{a\sigma} - \Sigma_{aa}(\omega)} + i0^+\right]^{-1} \tag{8}$$

where

$$\lambda_{ab} = \sum_{\mathbf{k}} \frac{V_a V_b}{2\sqrt{N_a N_b}} \sqrt{\frac{\phi(\mathbf{k})}{\phi^*(\mathbf{k})}} e^{-ik_x a} \left(\frac{1}{\omega - \epsilon_+(\mathbf{k}) + \mathbf{i0}^+} - \frac{1}{\omega - \epsilon_-(\mathbf{k}) + \mathbf{i0}^+}\right)$$

and

$$\lambda_{ba} = \sum_{\mathbf{k}} \frac{V_a V_b}{2\sqrt{N_a N_b}} \sqrt{\frac{\phi^*(\mathbf{k})}{\phi(\mathbf{k})}} e^{ik_x a} \left(\frac{1}{\omega - \epsilon_+(\mathbf{k}) + \mathbf{i0}^+} - \frac{1}{\omega - \epsilon_-(\mathbf{k}) + \mathbf{i0}^+}\right)$$

Upon linearization we observe that $\lambda_{ab} = \lambda_{ba} = 0$ [19] and thereby Eq. (8) can be written as

$$G^R_{bf\sigma}(\omega) = \left[\omega - \epsilon_{b\sigma} - \Sigma_{bb}(\omega) - \frac{V_{ab}V_{ba}}{\omega - \epsilon_{a\sigma} - \Sigma_{aa}(\omega)} + i0^+\right]^{-1} \tag{9}$$

where

$$\Sigma_{bb}(\omega) = -\frac{V_b^2}{D^2}\left\{\omega \ln\left(\frac{|\omega^2 - D^2|}{\omega^2}\right) + i\pi|\omega|\theta(D - |\omega|)\right\}$$

and

$$\Sigma_{aa}(\omega) = -\frac{V_a^2}{D^2}\left\{\omega \ln\left(\frac{|\omega^2 - D^2|}{\omega^2}\right) + i\pi|\omega|\theta(D - |\omega|)\right\}.$$

D is a high-energy cutoff of the order of the graphene bandwidth chosen according to the Debye prescription [12]. We assume also that $\mu \ll D$ where the band effects does not depend on the above cut-off. In the similar fashion we can also write down $G^R_{af\sigma}(\omega)$ and calculate the occupation of the spin dependent states of the impurity interacting with the A sublattice. Thereby, we can study the phase transition related to the magnetic moment formations and also the individual occupation dependence on V_{ab} and also on the relative values of V_a and V_b. As in [7], we observe a chemical potential dependence of the magnetic regions and occupation.

4. Results and discussion

In this section we present the phase diagram of the impurity coupled to the B sublattice as a function of the parameters $x = \Delta_b D/U$ and $y = (\mu - \epsilon_f)/U$ utilizing Eq. (9). A analogous phase diagram of the impurity coupled to the A sublattice can be obtained due to the similar nature of the impurities. The dimensionless hybridizations for the two impurities are given by $\Delta_\alpha = \pi V_\alpha^2/D^2$. For the sake of numerical calculation graphene is represented by a bandwidth $D = 7.0$ eV [12] and the lattice spacing $a = 0.14$ nm [20]. The dependence of the phase diagram on the chemical potential and also V_a, V_b and V_{ab} are shown.

In Fig. 2. we exhibit the phase diagram for $V_a/D = 0$, $V_b/D = 0.14$, $V_{ab}/D = 0.0$. As $V_{ab} = 0.0$ simplifies Eq. (9), we observe that the occupation does not depend on $\epsilon_{a\sigma}$. Hence, it demonstrates the single-impurity case in single-layer graphene. Similar situation should also be observed for the impurity coupled to A. The chemical potential dependence of the boundary can be observed as μ/D varies as following: 0.015 (solid line), 0.028 (dashed line), 0.073 (dotted line), 0.1 (dashed-dotted line) and 0.14 (dashed-double-dotted line). We observe that unlike the metallic case, the boundary is asymmetric around $y = 0.5$ and the magnetic region decreases with the increase in μ. This reveals the particle-hole symmetry breaking due to the presence of the localized state and also that the level magnetizes even when the impurity is above the Fermi level.

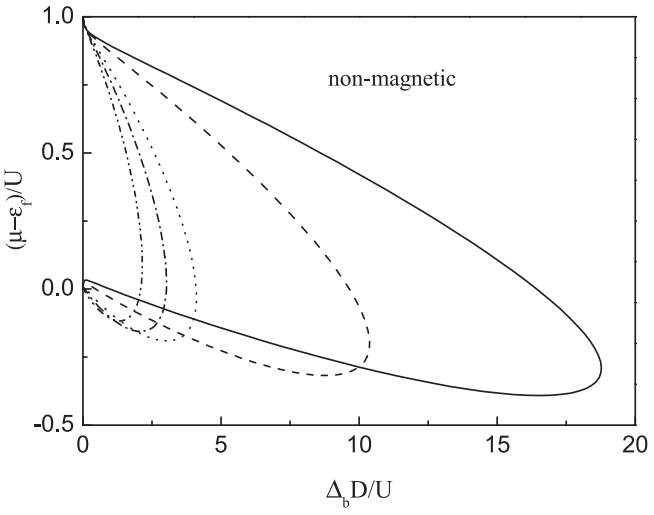

Fig. 2. Boundary between magnetic and non-magnetic phase in the variables $x = \Delta_b D/U$ and $y = (\mu - \epsilon_f)/U$ for $V_a/D = 0$, $V_b/D = 0.14$, $V_{ab}/D = 0.0$ and $\mu/D = 0.015$ (solid line), 0.028 (dashed line), 0.073 (dotted line), 0.1 (dashed-dotted line) and 0.14 (dashed-double-dotted line).

In the presence of the hybridization interaction between the adatom and the graphene A sublattice V_a and the interaction between the two impurities V_{ab} the boundary between the magnetic and non-magnetic states of the B sub-lattice are studied in Figs. 3–5 for two sets of the above interactions: (i) $V_a/D = 0.14$, $V_b/D = 0.14$ and (ii) $V_a/D = 0.14$, $V_b/D = 0.17$.

In Fig. 3, the phase diagram as a function of x and y is studied for $\mu/D = 0.015$. The boundary for set (i) with $V_{ab}/D = 0.014$ (black solid-line), $V_{ab}/D = 0.029$ (black dashed-line) and $V_{ab}/D = 0.043$ (black dotted-line) and that for set (ii) for $V_{ab}/D = 0.014$ (red solid-line), $V_{ab}/D = 0.029$ (red dashed-line) and $V_{ab}/D = 0.043$ (red dotted-line) are demonstrated in (a) $\epsilon_{a\sigma}/D = 0.0$, (b) $\epsilon_{a\sigma}/D = 0.014$, (c) $\epsilon_{a\sigma}/D = 0.029$, (d) $\epsilon_{a\sigma}/D = 0.071$, (e) $\epsilon_{a\sigma}/D = 0.11$ and (f) $\epsilon_{a\sigma}/D = 0.14$.

In Fig. 3(a) for $\mu > \epsilon_{a\sigma}$ we observe the symmetry to be different as compared to that in Fig. 2. The y-values attains values more than unity. The presence of the localized level occurs when the impurity level of the B sublattice is below the Fermi level. In Fig. 3(b), $\mu \sim \epsilon_{a\sigma}$, the boundary is symmetric around $y = 0.5$ when compared to the other cases and is very similar to the case of the metals. the x-values over which the localized moment exists is the least among all the cases considered. However, as $\mu < \epsilon_{a\sigma}$ in (c)–(f) the symmetry of the boundary changes and we observe negative values of y. Moreover, the x values gradually increases as we increase $\epsilon_{a\sigma}$. With the change is V_{ab} the magnetic phase decreases in all the cases. For, $\mu \ll \epsilon_{a\sigma}$ in (d)–(f) the nature of the boundaries are similar to each other and the local moment formation takes place for impurity levels much above the Fermi level. But the y values become more negative with the increase in V_{ab}. The effects of the impurity of the sublattice A, the interaction V_{ab} and the chemical potential on the impurity of the sublattice B are demonstrated.

In Fig. 4 the phase diagram of the sets (i) and (ii) are plotted for $\mu/D = 0.073$ for the same values of V_{ab} of Fig. 3 in (a) $\epsilon_{a\sigma}/D = 0.0$, (b) $\epsilon_{a\sigma}/D = 0.029$, (c) $\epsilon_{a\sigma}/D = 0.057$, (d) $\epsilon_{a\sigma}/D = 0.071$, (e) $\epsilon_{a\sigma}/D = 0.086$ and (f) $\epsilon_{a\sigma}/D = 0.14$. The distinction between the $\mu < \epsilon_{a\sigma}$ and $\mu > \epsilon_{a\sigma}$ symmetry and the symmetric nature for $\mu \sim \epsilon_{a\sigma}$ is preserved. Moreover it is can be noted that in Fig. 4(a)

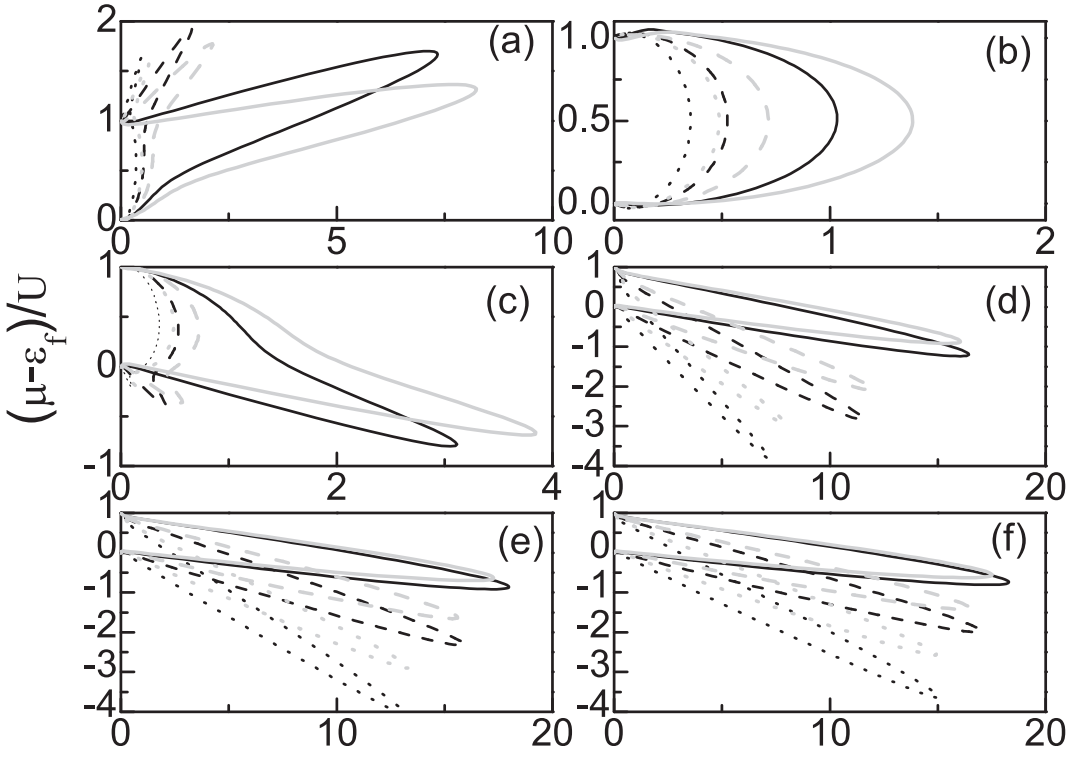

Fig. 3. Boundary between magnetic and non-magnetic phase in the variables $x = \Delta_b D/U$ and $y = (\mu - \epsilon_f)/U$ for $\mu/D = 0.015$ and for $V_a/D = 0.14$, $V_b/D = 0.14$, $V_{ab}/D = 0.014$ (black solid-line), $V_{ab}/D = 0.029$ (black dashed-line) and $V_{ab}/D = 0.043$ (black dotted-line) and $V_a/D = 0.14$, $V_b/D = 0.17$, $V_{ab}/D = 0.014$ (grey solid-line), $V_{ab}/D = 0.029$ (grey dashed-line) and $V_{ab}/D = 0.043$ (grey dotted-line) in (a) $\epsilon_{a\sigma} = 0.0$, (b) $\epsilon_{a\sigma}/D = 0.014$, (c) $\epsilon_{a\sigma} = 0.029$, (d) $\epsilon_{a\sigma} = 0.071$, (e) $\epsilon_{a\sigma} = 0.11$ and (f) $\epsilon_{a\sigma} = 0.14$.

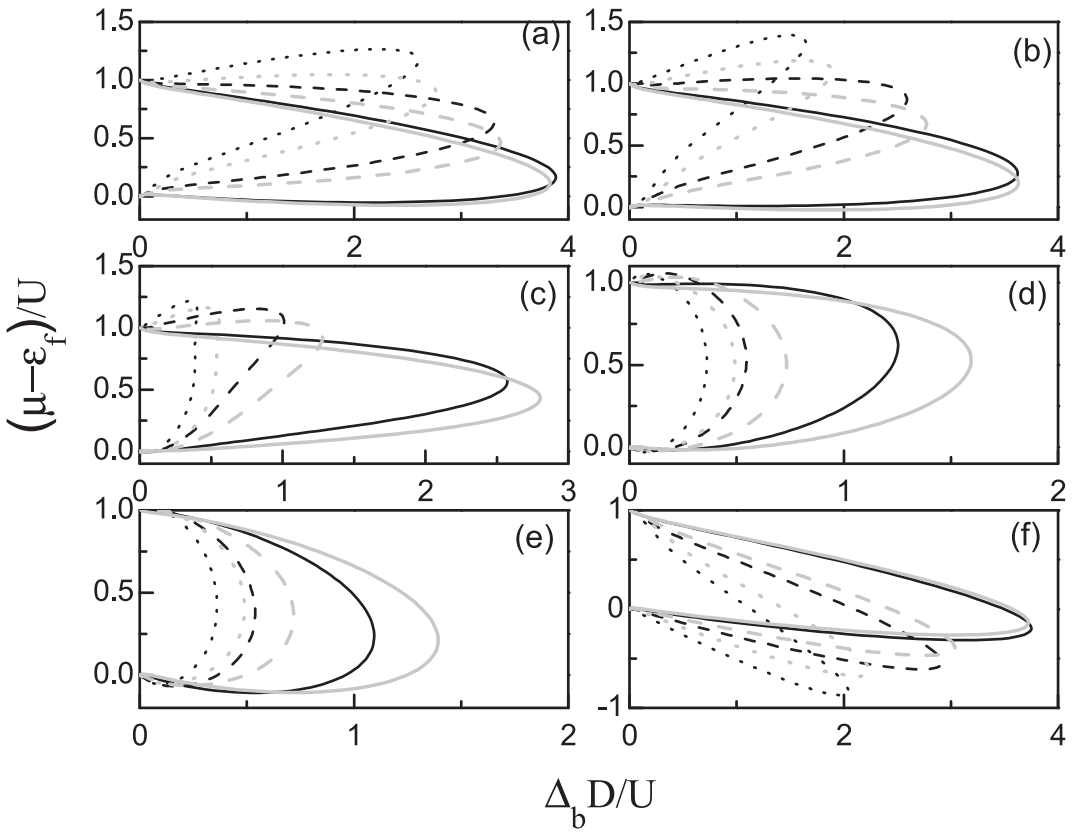

Fig. 4. Boundary between magnetic and non-magnetic phase in the variables $x = \Delta_b D/U$ and $y = (\mu - \epsilon_f)/U$ for $\mu/D = 0.073$ and for $V_a/D = 0.14$, $V_b/D = 0.14$, $V_{ab}/D = 0.014$ (black solid-line), $V_{ab}/D = 0.029$ (black dashed-line) and $V_{ab}/D = 0.043$ (black dotted-line) and $V_a/D = 0.14$, $V_b/D = 0.17$, $V_{ab}/D = 0.014$ (grey solid-line), $V_{ab}/D = 0.029$ (grey dashed-line) and $V_{ab}/D = 0.043$ (grey dotted-line) in (a) $\epsilon_{a\sigma}/D = 0.0$, (b) $\epsilon_{a\sigma}/D = 0.029$, (c) $\epsilon_{a\sigma}/D = 0.057$, (d) $\epsilon_{a\sigma}/D = 0.071$, (e) $\epsilon_{a\sigma}/D = 0.086$ and (f) $\epsilon_{a\sigma}/D = 0.14$.

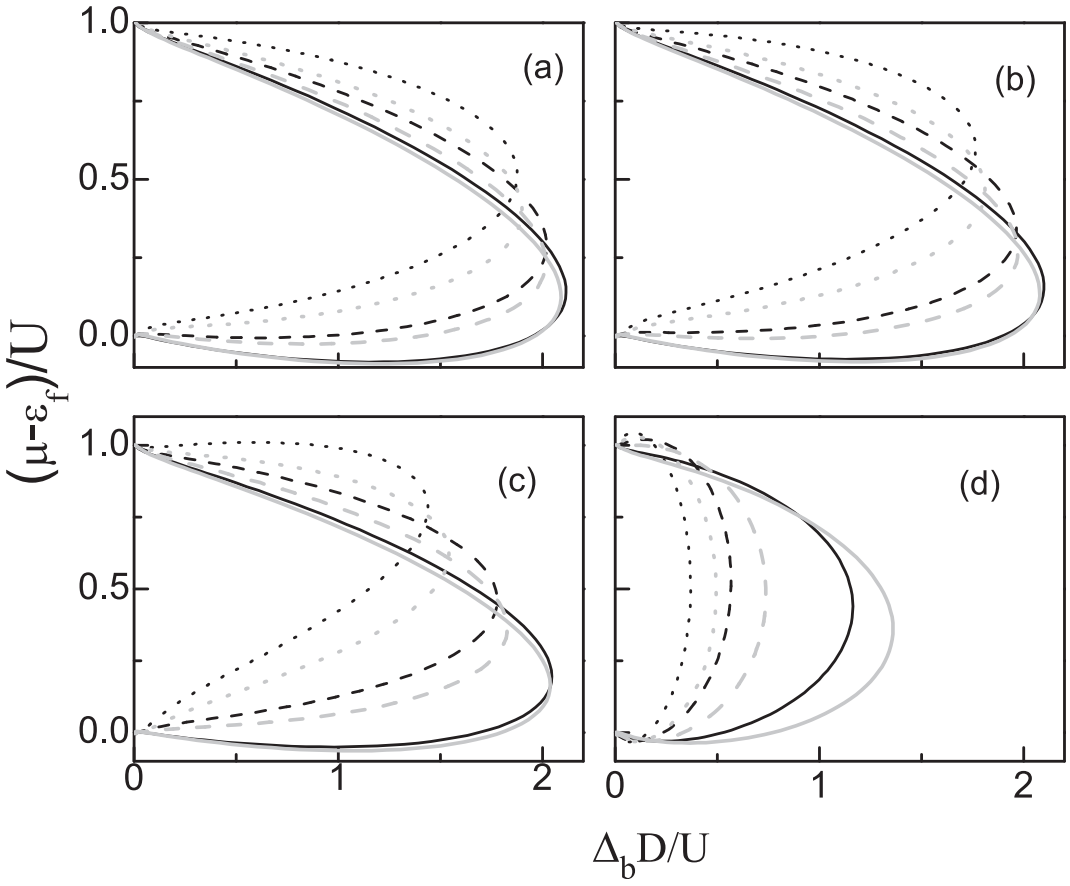

Fig. 5. Boundary between magnetic and non-magnetic phase in the variables $x = \Delta D/U$ and $y = (\mu - \epsilon_f)/U$ for $\mu/D = 0.14$ and for $V_a/D = 0.14$, $V_b/D = 0.14$, $V_{ab}/D = 0.014$ (black solid-line), $V_{ab}/D = 0.029$ (black dashed-line) and $V_{ab}/D = 0.043$ (black dotted-line) and $V_a/D = 0.14$, $V_b/D = 0.17$, $V_{ab}/D = 0.014$ (grey solid-line), $V_{ab}/D = 0.029$ (grey dashed-line) and $V_{ab}/D = 0.043$ (grey dotted-line) in (a) $\epsilon_{a\sigma} = 0.0$, (b) $\epsilon_{a\sigma}/D = 0.029$, (c) $\epsilon_{a\sigma} = 0.071$, and (d) $\epsilon_{a\sigma} = 0.14$.

the boundary is symmetric for $V_{ab} = 0.029$ for both the sets of hybridization values. Hence, apart from the chemical potential values, the interaction between the impurities in the two sublattices also modifies the symmetry of the boundary. Moreover, for $\mu > \epsilon_{a\sigma}$ we observe that V_{ab} tends to change the symmetry of the boundary line of the two phases. Hence, for these cases we will always have a value of V_{ab} which gives the symmetric phase, for e.g in (b) and (c) the values are $0.014 < V_{ab} < 0.029$. The magnetic phase decreases with an increase of V_{ab} in all the cases.

The division of the two phases for $\mu = 0.14$ is plotted as a function of the x and y in Fig. 5 for set (i) for the same values of V_{ab} of Fig. 3 in (a) $\epsilon_{a\sigma} = 0.0$, (b) $\epsilon_{a\sigma}/D = 0.029$, (c) $\epsilon_{a\sigma} = 0.071$ and (d) $\epsilon_{a\sigma} = 0.14$. Just like in Fig. 4, in this case also we observe the symmetric nature for $V_{ab} = 0.2$ for both the sets of hybridization values and for $\mu \sim \epsilon_{a\sigma}$. With the increase of μ we observe that the value of V_{ab} which gives the symmetric phase, for e.g in (b) and (c) the values are $0.029 < V_{ab} < 0.043$. As in this case, $\mu > \epsilon_{a\sigma}$ in (a)–(c) we have the same symmetry preserved for all of them where y values are less than unity and also that the level magnetizes even when the impurity is above the Fermi level.

In Fig. 6, the dependence of the occupation numbers $n_{a\uparrow}$ and $n_{a\downarrow}$ of the impurity of the sublattice A and $n_{b\uparrow}$ and $n_{b\downarrow}$ of the impurity of the sublattice B on the chemical potential μ are plotted for (a) $\epsilon_f/D = 0.029$, $U_a/D = U_b/D = 0.043$, $V_a/D = V_b/D = 0.14$, $V_{ab}/D = 0.0$ (solid line), 0.014 (dashed line), 0.029 (dotted line) and 0.043 (dashed-dotted line) (b) $\epsilon_f/D = 0.029$, $U_a/D = 0.043$, $U_b/D = 0.071$, $V_a/D = V_b/D = 0.14$, $V_{ab}/D = 0.0$ (solid line), 0.029 (dashed line) and 0.043 (dotted line) and (c) $\epsilon_f/D = 0.029$, $U_a/D = 0.043$ $U_b/D = 0.071$, $V_a/D = 0.14$, $V_b/D = 0.17$, $V_{ab} = 0.0$ (solid line), 0.029 (dashed line) and 0.043 (dotted line). In Fig. 6(a) we observe the occupations of two similar impurities in the two sublattices of the single layer graphene when U_α and the hybridization V_α are same we observe the occupations of $n_{\alpha\sigma}$ to be the same. Hence both are represented in black. The $V_{ab} = 0$ case (two independent similar impurities) is in agreement with our earlier study [13]. With finite values of the interaction between the impurities we observe a change in behavior where $n_{\alpha\sigma}$ is below 0.5 for chemical potential less than the impurity level energy and it has values above 0.5 when $\mu > \epsilon_f$. The region of local moment formation moves away from the non-interacting case as we increase V_{ab}. The $n_{\alpha\sigma}$ values and also the magnetization values decreases as we increase the interaction V_{ab}. In the case for $U_a \neq U_b$ the difference arises in the magnetization values and also in the chemical potential values over which we observe the local moment formation. For $V_{ab} = 0$ we observe that the region over which the local moments exists for impurity of the B sublattice is nearly double that of A as $U_b > U_a$. With finite values of V_{ab} the above difference nearly goes to zero but unlike the previous case the magnetization values vary, magnetization of the A sublattice is less than that of the B sublattice. In (c) we observe as $V_a \neq V_b$ the loops that represent the local magnetic moments of the A and B impurities tend to move away from each other and is formed for higher values of μ when compared to that (a) and (b).

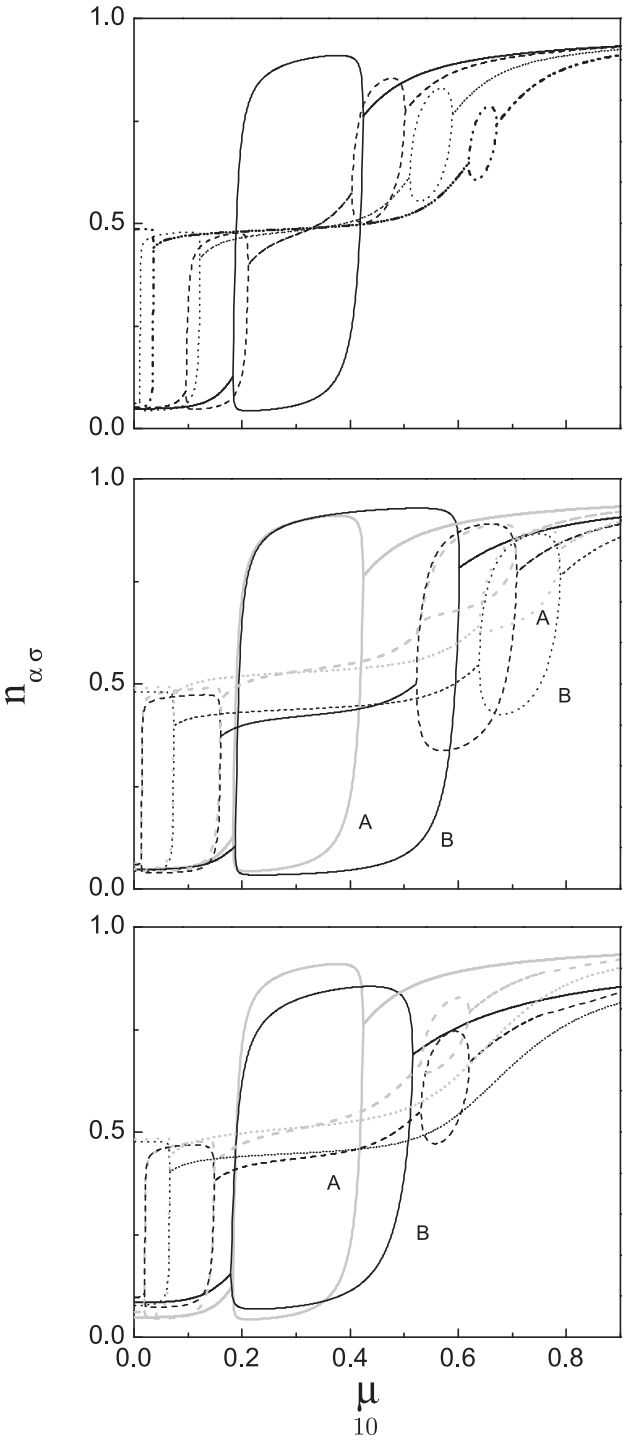

Fig. 6. $n_{a\sigma}$ (grey line) and $n_{b\sigma}$ (black line) vs μ for (a) $\epsilon_f/D = 0.029$, $U_a/D = U_b/D = 0.043$, $V_a/D = V_b/D = 0.14$, $V_{ab}/D = 0.0$ (solid line), 0.014 (dashed line), 0.029 (dotted line) and 0.043 (dashed-double-dotted line) (b) $\epsilon_f = 0.029$, $U_a/D = 0.043$, $U_b/D = 0.071$, $V_a/D = V_b/D = 0.14$, $V_{ab}/D = 0.0$ (solid line), 0.029 (dashed line) and 0.043 (dotted line) and (c) $\epsilon_f/D = 0.029$, $U_a/D = 0.043$ $U_b/D = 0.071$, $V_a/D = 0.14$, $V_b/D = 0.17$, $V_{ab} = 0.0$ (solid line), 0.029 (dashed line) and 0.043 (dotted line). In (a) $n_{a\sigma} = n_{b\sigma}$ and they are represented in black.

5. Conclusion

In summary, we study the effect of the interaction between the pair of neighboring magnetic atoms in the different sublattices of a single-layer graphene sheet. The local moment formation depends highly on the chemical potential. The asymmetric nature of the phase diagram is very prominent. However, the boundary between the magnetic and the non-magnetic phases gets modified with hybridization parameter and also the interaction between the impurities. Unlike the single-impurity case, we observe the symmetric nature of the boundary for certain values of the chemical potential and V_{ab} as observed in metals. the magnetization values and the region over which the local moment formation takes place decreases with V_{ab}. We also observe that local moment formation occurs even when the impurity is above the Fermi level. The occupation numbers are also sensitive to V_{ab} and changes appreciably with it. The effect of the Coulomb interaction and also the hybridization parameter are also exhibited.

Acknowledgement

The authors acknowledge financial support from the Brazilian funding agency, CNPq.

References

[1] K.S. Novoselov, Science 306 (2004) 666;
K.S. Novoselov et al., Nature (London) 438 (2005) 197;
Y. Zhang et al., Nature (London) 438 (2005) 201;
A.K. Geim, K.S. Novoselov, et al., Nat. Mater. 6 (2007) 183.
[2] B. Uchoa, T.G. Rappoport, A.H. Castro Neto, Phys. Rev. Lett. 106 (2011) 016801.
[3] T.O. Wehling, M.I. Katnelson, A.I. Lichtenstein, Chem. Phys. Lett. 476 (2009) 125.
[4] D.M. Eigler et al., Nature 344 (1990) 524.
[5] A.V. Krasheninnikov, P.O. Lehtinen, A.S. Foster, P. Pyykko, R.M. Nieminen, Phys. Rev. Lett. 102 (2009) 126807.
[6] H. G-Herrero, J.M. G-Rodriguez, P. Mallet, M. Moaied, J.J. Palacios, C. Salgado, M. M. Uqeda, J.Y. Veuillen, F. Yndurain, I. Brihuega, Science 352 (2016) 437.
[7] F.M. Hu, L. Kou, T. Frauenheim, Sci. Rep. 5 (2015) 8943.
[8] S. LeBohec, J. Talbot, E.J. Mishchenko, Phys. Rev. B 89 (2014) 045433.
[9] T.O. Wehling, A.V. Balatsky, M.I. Katnelson, A.I. Lichtenstein, K. Scharnberg, R. Wiesendanger, Phys. Rev. B 75 (2007) 125425.
[10] P.W. Anderson, Phys. Rev. 124 (1961) 41.
[11] S. Alexander, P.W. Anderson, Phys. Rev. 133 (1964) A1594.
[12] B. Uchoa, V.N. Kotov, N.M.R. Peres, A.H. Castro Neto, Phys Rev. Lett. 101 (2008) 026805.
[13] A. Ghosh, H.O. Frota, Physica B 407 (2012) 1170.
[14] A.C. Hewson, The Kondo problem to Heavy Fermions, Cambridge Univ. Press, New York, 1997.
[15] G.D. Mahan, Many Particle Physics, Kluwer Academic, New York, 2000.
[16] A.L. Fetter, J.D. Walecka, Quantum Theory of Many-Particle Systems, Dover, New York, 2003.
[17] A.A. Abrikosov, L.P. Gorkov, I.E. Dzyaloshinski, Methods of Quantum Field Theory in Statistical Physics, Dover, New Jersey, 1975.
[18] A. Ghosh, J.W.M. Pinto, H.O. Frota, J. Magn. Res. 227 (2013) 87.
[19] T. Ando, in: T. Enoki, T. Ando (Eds.), Physics and Chemistry of Graphene: Graphene to Nanographene, Pan Stanford Publishing, 2013.
[20] S. Das Sarma, S. Adam, E.H. Hwang, E. Rossi, Rev. Mod. Phys. 83 (2011) 407.